New Binding Specificities Derived from Min-23, a Small Cystine-Stabilized Peptidic Scaffold†

Christelle Souriau,‡ Laurent Chiche,§ Robert Irving,‡ and Peter Hudson*,‡

CRC for Diagnostics at CSIRO Health Sciences and Nutrition, 343 Royal Parade, Parkville, Victoria, 3052 Australia, and Centre de Biochimie Structurale, UMR5048 CNRS-Université Montpellier I, UMR554 INSERM-Université Montpellier I, Faculté de Pharmacie, 15 avenue Charles Flahault, BP 14491, 34093 Montpellier-Cedex 5, France

Received August 26, 2004; Revised Manuscript Received March 15, 2005

ABSTRACT: The randomization of both internal and surface residues in small protein domains followed by selection from a display library is emerging as a powerful strategy to obtain novel binding specificities. Small and stable scaffold motifs observed in disulfide-rich proteins are attractive because they are small, stable, and accessible to chemical synthesis. The elementary structural motif found in the squash trypsin inhibitor EETI-II (*Ecballium elaterium* trypsin inhibitor) is the cystine stabilized beta-sheet (CSB) motif, found in nearly 50% of all known small disulfide-rich protein families. We have used Min-23, a short 23-residue peptide containing the CSB motif and shown to be a stable autonomous folding unit and one of the smallest scaffolds described to date, as a scaffold for selection of new binding ligands. We demonstrate that the core CSB motif in Min-23 is permissive to loop insertion, using peptide epitopes from hemagglutinin (HA) and Gla-protein (E). A phage library of more than 10^8 different clones has been constructed by insertion of a randomized sequence on a β-turn of the Min-23 peptide. The selection of this library on a variety of 7 different targets allowed the isolation of 21 new specific binders, confirming the potential of Min-23 as a scaffold for the development of new ligands. The derived library is able to provide a wide range of novel compounds with possible applications in various biological and pharmaceutical areas.

Large repertoires of proteins have been extensively used to select ligand-binding molecules for a variety of applications (*1*). These combinatorial libraries are typically displayed on the surface of filamentous phage, which allow rapid isolation of new ligands through several selection cycles against target molecules. Antibodies, usually as their Fab and scFv fragments, were among the first protein libraries developed, and many high-affinity antibodies have been selected (*1*−*3*). However, the large antigen-binding surface on antibodies can prevent their binding to a number of targets, and smaller molecules such as peptides can sometimes provide higher affinity binding reagents that better penetrate the target molecule. Linear peptide libraries have been developed and successfully selected for high-affinity binders (*4*−*6*). However, imposing some structural constraints can offer affinity advantages during the selection of new specificities (*7*). Short loops were created by bringing together two segments of the same polypeptide with a disulfide bond. Disulfide-constrained libraries have proven very successful for selection of new binders (*8*, *9*). Alphaconotoxin, a small disulfide-constrained protein, comprising two disulfide bonds was mutated and displayed as a phage library (*10*). Ligands selected from libraries may require only a few critical residues that participate actively in binding, while the remaining residues provide adequate structure and conformation, effectively forming a scaffold on which amino acids can be inserted and randomized to create new specificities. Antibodies can be considered a stable scaffold which supports the binding region comprising up to six constrained peptide loops, known as the complementary determining regions (CDRs). As an alternative to single-loop peptide libraries, a number of different scaffolds have been developed to display a variety of peptide loops, both in number and size (*11*, *12*). The most successful scaffolds reported so far include the Z-domain of protein A (*13*, *14*), tendamistat (*15*), Kunitz domain (*16*), fibronectin type III domain (*17*, *18*) and lipocalin (*19*, *20*), cellulose binding domain (CBD) (*21*, *22*), basic pancreatic trypsin inhibitor (BPTI) (*23*), the variable domain of CTLA-4 (*24*), or the thermostable carbohydrate binding module CBM4-2 (*25*). Binding proteins derived from these scaffolds have different intrinsic characteristics making them suitable for different applications depending on their properties. For example, biosensors require exceptional in vitro stability, whereas therapeutic administration requires special formulation to achieve the desired in vivo pharmacokinetics and bioavailability. It is therefore likely that future applications will need a wide range of different scaffolds with various characteristics.

The natural protein repertoire seems to comprise only a limited number of folds that have probably been optimized through evolution for the best compromise between stability and efficiency. In particular, remarkably stable core scaffolds made of small disulfide-rich motifs have been observed in proteins with very diverse origins and functions. For example,

† This work was supported by the Centre Informatique National de l'Enseignement Supérieur, Montpellier.

* To whom correspondence should be addressed. Telephone: +61 3 9662 7312. Fax: +61 3 9662 7313. E-mail: peter.hudson@hsn.csiro.au.

‡ CRC for Diagnostics at CSIRO Health Sciences and Nutrition.

§ Université Montpellier I.

10.1021/bi0481592 CCC: $30.25
Published on Web 04/21/2005

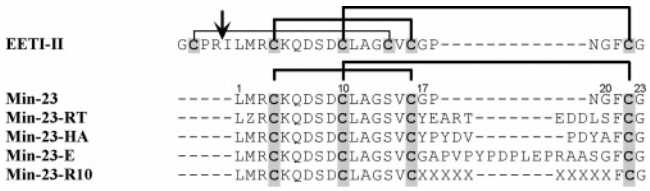

FIGURE 1: Sequences of EETI-II, Min-23 (*39*), Min-23-RT (*40*), Min-23-HA, Min-23-E, and Min-23 library (Min23-R10). All sequences have been aligned onto the longest one (Min-23-E), and dashed are inserted in shorter sequences. The active site in EETI-II is highlighted with an arrow. The numbering refers to the Min-23 sequence and not to wild knottins. The disulfide connectivity is shown as lines and gray shaded boxes in Min-23 and its variants. The additional disulfide bridge in the EETI-II knottin is shown as thin lines. The X letters refer to randomized amino acids in the Min-23 combinatorial library, and the Z letter refers to nor-leucine in Min-23-RT.

the serine proteinase inhibitors from the squash family, with only about 30 amino acids and three disulfide bridges, are among the smallest rigid structures (*26*). They are composed of a triple-stranded antiparallel β-sheet, a 3_{10} helix, two β-turns, and a specific disulfide arrangement in which one disulfide bridge penetrates the macrocycle created by the two other disulfide bridges and interconnecting backbones (*27*−*32*). This particular arrangement of three disulfide bridges is present in many proteins with no apparent evolutionary relationship, the knottins, including protease inhibitors, toxins from plants and animals, hormone-like peptides, or insect antimicrobials (*33*). The replacement of the inhibitory loop of the knottin EETI-II[1] (*27*) by either 13 residues or 17 residues resulted in novel fusion proteins that were correctly folded, suggesting that knottins can provide interesting scaffolds for the construction of constrained random libraries (*12*, *34*, *35*). However, the location of the active site in knottins varies between families, and structural alignments and folding experiments suggested that only two out of three disulfide bridges and the small triple-stranded β-sheet are highly conserved and define a common elementary structural motif (*36*−*38*). This motif, called the cystine-stabilized β-sheet (CSB) motif, was shown to be an autonomous folding unit (*39*). Although the CSB motif has never been observed alone in nature, it appears to be one of the most widespread disulfide-rich motifs probably due to its high intrinsic stability (*39*). Indeed, a minimal 23-residue peptide (Min-23), containing the CSB motif and lacking the inhibitory loop, was designed from EETI-II, synthesized, and subjected to NMR analyses which demonstrated a correct native-like fold and a high stability (Tm $\sim$ 100 °C) (*39*). Sequences of EETI-II and Min-23 are displayed in Figure 1, and a schematic representation of Min-23 is shown in Figure 2.

In this paper, we show that the Min-23 peptide is an effective small stable scaffold for obtaining new active molecules via phage display and selection. First, fusion proteins were made by insertion of known sequences onto the Min-23 peptide. Then a library of 2.8×10^8 clones was constructed by insertion of 10 random amino acids into the second β-turn of Min-23. This library was expressed on phage and selected on seven different targets. Selected clones were analyzed for their binding affinity and specificity, and

[1] Abbreviations: CSB, cystine-stabilized beta-sheet; DTT, dithiothreitol; EETI, *Ecballium elaterium* trypsin inhibitor; HA, haemagglutinin.

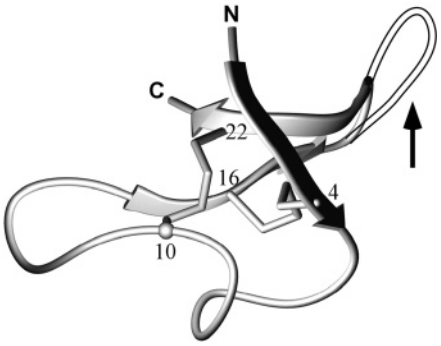

FIGURE 2: Schematic representation of Min-23. Cysteines are shown as sticks and are numbered according to the Min-23 numbering. The triple-stranded β-sheet is displayed as flat arrows. The position of the inserted loops in Min-23-RT, -HA, -E, and -R10 is indicated by a double-line drawing and a black arrow.

21 specific clones with various binding properties were obtained.

MATERIALS AND METHODS

Bacterial Strain. The following bacterial strain was used: TG1: K12, Δ (*lac-pro*), *sup*E, *thi*, *hsd*D5/F′*tra*D36, *pro*A$^+$ B$^+$, *lac*I^q, *lac*ZΔM15.

Construction of the Chimeras Min-23-Ha and Min-23-E. Phage expressing Min-23 fused to the sequence HA and phage expressing Min-23 fused to the sequence E were prepared by PCR amplification using the following primers.

For Min-23-HA, we used primers G1, 5′TTACTCGCGG CCCAGCCGGCCATGGCCGCCGCCCTGATGCGTTGC-AAACAGGAT 3′; G2, 5′CTGATGCGTTGCAAACAG-GATAGCGATTGCCTGGCGGGCAGCGTGTGC 3′; G3, 5′ATAATCTGCGGCCGCGCCGCAGAACGCATAATC-CGGCACATCATACGGATAGCACACGCTGCCCGCC-AG 3′.

For Min-23-E, we used primer G1 and G2 as above and primers G4, 5′GCTCGCCGCACGCGGTTCCAGCGGATC-CGGATACGGCACCGGCGCGCCGCACACGCT GCCCG-CCAG 3′, and G5, 5′ATAATCTGCGGCCGCGCCGCA-GAAGCCGCTCGCCGCACGCGGTTC 3′.

PCR fragments were cloned into the phagemid vector pHFA$_{SAC}$ (*41*) using its *Sfi*I and *Not*I sites. Ligation products were electroporated into *Escherichia coli* TG1 cells for phage production.

Construction of the Library. A phage display library expressing Min-23 with 10 random amino acids inserted between residues 16 and 20 of Min-23 was prepared by PCR amplification using the following primers: G6755, 5′CT-GATGCGTTGCAAACAGGATAGCGATTGCCTGGCGGG-CAGCGTGTGC 3′; G6767, 5′GCCGCAGAAMNNMN-NMNNMNNMNNMNNMNNMNNMNNMNNGCACA-CGCTG CCCGCCAG 3′; G1, 5′TTACTCGCGGCCCAGC-CGGCCATGGCCGCCGCCCTGATGCGTTGCAAACA-GGAT 3′; G9, 5′ATAATCTGCGGCCGCGCCGCAGAA 3′.

PCR fragments were cloned into the phagemid vector pHFA$_{SAC}$ (*41*) using its *Sfi*I and *Not*I sites. Ligation products were electroporated into *Escherichia coli* (*E. coli*) TG1 cells for phage production. The number of transformants after electroporation was calculated and used to determine the size of the library.

Selection of the Library. Seven different proteins were used as targets in the selection of the library. The malarial apical

membrane antigen 1 (AMA-1) was kindly supplied by Dr. M. Foley, School of Biochemistry, La Trobe University, Australia. The 60 kDa cytosolic domain of the 70 kDa outer membrane translocase receptor from human mitochondria (Tom70) was kindly supplied by Dr. N. Hoogenraad, School of Biochemistry, La Trobe University, Australia. The antibodies anti-AMA-1 clone 5G8 (5G8 Ab) and clone 1F9 (1F9 Ab) were kindly supplied by Dr. R. Anders, School of Biochemistry, La Trobe University, Australia. The anti-EBV antibody (anti-capsid protein gp 125 of Epstein Barr Virus) clone L2 (anti-EBV Ab), the anti-Nef antibody (anti-aa 31−50) (anti-Nef Ab), and the HIV-1 Nef protein were purchased from Advanced Biotechnologies Inc., Columbia, MD.

Colony Blot. E. coli TG1 bacteria harboring the plasmid $pHFA_{SAC}$ were grown at 37 °C and IPTG-induced before lysis. Periplasmic fractions were blotted onto nitrocellulose filters and probed with an anti-Flag antibody. Fd-phage were produced using the phagemid vector as described (*42*); all phage were grown under the same conditions and in parallel with control phage displaying irrelevant protein. Phage concentration was measured by bacterial infection. Display of recombinant protein was checked by ELISA and Western blot. For ELISA, dilutions of phages were coated in 96-well plates and revealed with an anti-pIII antibody and in parallel with an anti-Flag antibody. For Western blot, dilutions of phages were subjected to polyacrylamide gel electrophoresis and transferred into nitrocellulose membranes. Membranes were then revealed with an anti-pIII antibody and in parallel with an anti-Flag antibody. For ELISA screenings, small-scale preparations of phage were used. Bacterial clones were grown as previously described (*42*) but in small a volume of 200 μL in 96-well plates. After poly(ethylene glycol) 8000 (PEG) precipitation, phage were finally resuspended in 100 μL of PBS.

ELISA. For detection of protein expressed on phage, dilutions of phage were coated on 96-well plates and revealed with an anti-pIII antibody, with an anti-E antibody, with an anti-HA antibody, or with an anti-Flag antibody. To analyze the binding of peptides expressed on phage on target protein, target proteins were coated on 96-well plates at a concentration of 0.5−1 μg/well. After blocking with 4% dry milk in PBS for 2 h, phages diluted in 2% dry milk in PBS were incubated for 1 h. Washes were performed with PBS and bound phage were revealed with an anti-fd antibody linked to biotin and an HRP−streptavidin conjugate. For competition experiments, different concentrations of competitors, such as the antibody anti-AMA-1 5G8 (5G8 Ab) or the antibody anti-AMA-1 1F9 (1F9 Ab), were mixed with phage for 30 min at room temperature before incubation with the target protein in the 96-well plates. For analysis of DTT sensitivity, phages were incubated with various concentrations of DTT for 30 min at room temperature before incubation with the target protein in the 96-well plates.

Expression of Recombinant Proteins. Selected clones were produced as recombinant proteins in fusion with the maltose-binding protein (MBP) using the pMal-E vector (New England Biolabs). Subcloning into this vector was performed after PCRs of the insert with the primers G33, 5′ TCCCAAGCTTGCACTCTAGCCGCA GAA 3′, and G34, 5′GGATCCTCTAGAATGGCCGCCGCCCTGATGCGTTGCAAACAGGATAGC 3′.

The PCR fragments were cloned into the pMal-E vector using the *Xba*I and *Hind*III sites. Recombinant proteins were expressed and purified as described (*43*). Briefly, proteins were expressed as fusion protein with the MBP and isolated from the periplasmic fraction. Proteins were purified by affinity chromatography using amylose−sepharose resin and elution with maltose as described (*43*).

Biosensor Binding Analysis. A BIAcore 1000 biosensor (Biacore AB, Uppsala Sweden) was used to measure the interaction between selected Min-23 binders and target antigen. The anti-EBV antibody was immobilized onto a CM5 sensor chip (700 RU) using the standard NHS− EDC coupling procedures via amine groups in 10 mM sodium acetate buffer, pH 4.5, at 25 °C and 5 μL/min flow rate. The binding experiments were performed in 10 mM Hepes, 0.15 M NaCl, 3.4 mM EDTA, and 0.005% surfactant P20, pH 7.4, at 25 °C and a constant flow rate of 5 μL/min. Regeneration of the anti-EBV antibody surface was achieved by running the dissociation reaction to completion before the next injection of analyte. The kinetic rate constants k_a and k_d were determined at each of the five concentrations (12.3−204 nM) using the fitting algorithm for 1:1 Langmuir binding (simultaneous fitting of k_a and k_d) model as described in BIAevalution 3.0.2.

Molecular Modeling. Structure calculations and displays were performed on a Linux workstation. Figures of structures were produced with the MOLMOL (*44*) and POV-Ray (http://www.povray.org) programs. The MODELLER program (*45*) was used to build initial models from the Min-23 solution structure (*39*) and the clone sequences. These initial models were submitted to molecular mechanics energy refinement with the sander module of the AMBER 7 program (*46*), using the all-atom parm94 force field (*47*) and the GB/SA implicit solvation system (*48*, *49*). Five thousand steps of energy minimization were first carried out with 1 kcal mol^{-1} positional restraint on the backbone atoms of the unchanged Min-23 scaffold. This is to allow the newly introduced loops to adapt to the Min-23 scaffold, still avoiding unrealistic deviation of the scaffold due to poor initial conformations of the loops. All intramolecular noncovalent interactions were computed by setting the nonbonded cutoff at 99 Å. The Generalized Born model was used to compute the polar contribution to the solvation free energy, using the parameters from Tsui and Case (*48*). Nonpolar contribution to the solvation free energy was computed as surften × SA, where surften is a surface tension of 0.005 kcal mol^{-1} $Å^{-2}$ and SA is the accessible surface area. Then, to sample the conformational space available to the molecules, 500 ps-long molecular dynamics simulations were performed. During the molecular dynamics runs, the covalent bond lengths were kept constant by applying the SHAKE algorithm (*50*) allowing a 1.5 fs time step to be used. The system was coupled to a heat bath of temperature $T_0 = 298$ K (*51*), using a temperature relaxation time $t_T = 0.2$ ps. Conformations were saved every 5 ps, and the conformation closest to the average conformation was used for analysis and display.

RESULTS

Modification of Min-23 by Insertion of New Sequences into a Surface Loop. Expression of the Protein Chimeras

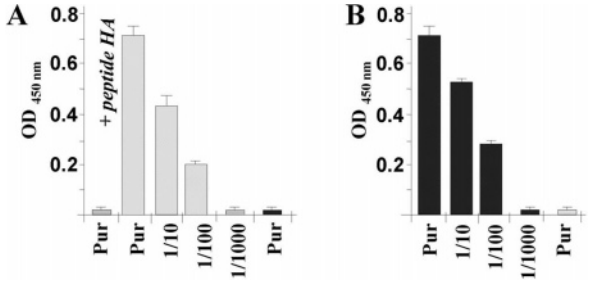

FIGURE 3: Analysis of binding specificity of phages displaying Min-23 chimeras by ELISA. Phage-Min23-HA (gray bars) and phage-Min23-E (black bars) were immobilized at different dilutions and were detected with (A) an anti-HA mouse antibody and (B) an HRP-conjugated anti-E mouse antibody. Competition was performed by incubating the peptide HA with the phage-Min23-HA. Experiments were performed in triplicate, and error bars represent ±SD.

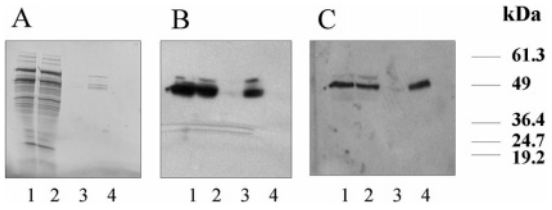

FIGURE 4: Analysis of fusion protein MBP−Min-23-HA after recombinant expression in *E. coli*. (A) SDS−PAGE 10% acrylamide. (B) Western blot developed with an anti-MBP antibody. (C) Western blot revealed with an anti-HA antibody. Columns 1 and 2: periplasmic fraction before purification on amylose resin. Column 3: wash fraction after incubation on amylose resin. Column 4: fraction after elution from amylose resin with maltose.

Min-23-HA and Min-23-E on the Surface of Phage. Sequence alignment and structural analyses showed a great variability in the size of the last loop or β-turn of CSB-containing proteins, and we predicted this would be an appropriate permissive site for introduction of novel loop sequences. The core CSB motif is stabilized by two disulfide bridges and a β-sheet, thus, exposing a β-turn for loop manipulation, that is, residues 17−20 in Min-23 (Figures 1 and 2). The Phe^{21} was kept unchanged because it is predicted to stabilize the CSB motif through hydrophobic interactions with Leu^{1} (*27*, *39*). To verify that new sequences could be inserted onto Min-23 at this position, two protein chimeras were created by inserting known sequences of different sizes in replacement of residues 17−20 (Figure 1), the sequence HA (YPYDVPDYA) derived from an epitope of the hemagglutinin protein of human influenza virus (*52*) and the sequence E (GAPVPYPDPLEPRAASG) derived from an epitope from the human bone Gla-protein (*53*). The resulting chimeras Min-23-HA and Min-23-E were expressed on the surface of the filamentous phage and tested by ELISA to determine whether chimeras could still be recognized by their corresponding antibodies anti-HA and anti-E (Figure 3). The antibody anti-HA bound specifically onto the phage Min-23-HA as well as the antibody anti-E on the phage Min-23-E with both ELISA signals depending on the concentration of phage. Furthermore, addition of the soluble peptide HA was able to completely inhibit the binding of the antibody anti-HA when it was mixed with the phage Min-23-HA, thus, confirming the specificity of the binding.

Expression of the Protein Chimeras Min-23-HA and Min-23-E as Fusion Proteins. Min-23-HA and Min-23-E were expressed as soluble, periplasmic fusion proteins by attachment to the C-terminus of *E. coli* maltose-binding protein (MBP). It had been previously reported that the oxidation conditions in the periplasm allow the formation of correctly folded and fully functional fusion of MBP with another CSB protein (EETI-II) in high yields (*34*). Recombinant proteins were analyzed before and after purification by affinity chromatography on amylose resin. SDS−PAGE under non-reducing conditions and Western blot using an anti-MBP antibody, an anti-HA antibody, or an anti-E antibody were performed (Figure 4). The fusion proteins MBP-Min-23-HA and MBP-Min-23-E were not degraded, and immunoblotting showed a soluble product of the expected size of 49 kDa, detected using both antibodies specific for the MBP tag and anti-HA or anti-E antibodies. Similar yields were obtained with the recombinant protein MBP−Min-23 suggesting that introduction of the new sequences HA or E onto the Min-23 scaffold did not significantly alter the expression level and that these new introduced sequences are well-tolerated.

The binding of these recombinant fusion proteins to their respective antibody was analyzed by ELISA, and specific binding was observed with soluble MBP-Min-23-HA and MBP−Min-23-E, but not with the control MBP−Min-23 (data not shown). These results clearly indicate that new sequences can be introduced onto Min-23 at the selected position and that the 9-residue and the 17-residue sequences are specifically recognized by their specific antibodies when displayed on the Min-23 scaffold.

Construction of a Min-23 Phage Library with Diversity in an Exposed Loop. A phage display library termed Min-23-R10 was constructed by PCR using a set of degenerate primers to amplify Min-23 and replace residues 17−20 by 10 random residues. The amplified Min-23 repertoire was cloned into the phagemid vector pHFASAC, and the number of colonies obtained after electroporation yielded a theoretical library size of 2.8×10^8 unique variants. To confirm library diversity, 30 individual clones were sequenced, and indeed the observed residue frequency was similar to that predicted (data not shown), although residues V, L, and S were slightly over-represented as has been observed in other phage display libraries (*54*). To assess the proportion of clones that expressed detectable Min-23 proteins, 40 individual clones were subjected to small-scale bacterial culture with IPTG induction, followed by analysis of periplasmic fractions on dot-blot using an anti-Flag antibody (data not shown). Out of 40 clones, 29 demonstrated the expected expression levels of Min-23 variants, indicating that the library contains at least 72.5% of clones which display surface proteins.

Selection of the Library. A well-characterized antibody (5G8 Ab) with specificity to the malarial antigen AMA-1 was chosen as the first target to select the Min-23 library. Previous selection of a 20-residue linear-peptide phage display library on the 5G8 Ab had identified that a consensus binding sequence of just three residues, AYP, was sufficient to bind effectively to 5G8 Ab (*55*). After the third round of selection of the Min-23 phage library on 5G8 Ab, binding was tested by phage ELISA. Clones were randomly picked from the selected fraction and used for a small-scale preparation of phage. Ninety percent of the clones showed specific binding to the antibody 5G8 with no detectable binding to the protein control, BSA. Fourteen unique clones

Min-23	LMRCKQDSDCLAGSVC**GP------NG**FCG
Min-23-R10	LMRCKQDSDCLAGSVC**XXXXXXXXXX**FCG
A	
R1	LMRCKQDSDCLAGXVC**VPVMPPMRXD**FCG
R2	LMRXKQDSDCLAGSVCTMFGFIVL.VLRRGRRL.R...XSR
R3	LMRCKQDSDCLAGSVC**WAADASGFAF**FCG
R4	LMRCKQDSDCLAGSVC**WLGGCGDVSL**FCG
R5	LMRCKQDSDCLAGSVC**APVCLLLLFR**FCG
R6	LMRCKQDSDCLAGSVC**LFLLLGSTLV**FCG
R7	LMRCKQDSDCLAGSVC**SPPPGFEFA.F**CG
R8	LMRCKQDSDCLAGSVC**YPYDVPDYAF**CG
R9	LMRCKQDSDCLAGSVC**L.LIVHLRRR**FCG
B	
S17E2	LMRCKQDSDCLAGSVC**LHYSYPVADP**FCG
S17E3	LMRCKQDSDCLAGSVC**QGQSYPDXVV**FCG
S17E8	LMRCKQDSDCLAGSVC**PWSYPPVXES**FCG
S17E9	LMRCKQDSDCLAGSVC**AVAYPVVDXD**FCG
S22E2	LMRCKQDSDCLAGSVC**SVSYPSE**FCG
S22E4	LMRCKQDSDCLAGSVC**AVAYPVVED**FCG
S22E5	LMRCKQDSDCLAGSVC**PFAYPVXPPP**FCG
S22E6	LMRCKQDSDCLAGSVC**PPVSVAYPEP**FCG
S22E7	LMRCKQDSDCLAGSVC**PWSYPVQESP**FCG
S22E8	LMRCKQDSDCLAGSVC**LAPAYPLPPD**FCG
S22E9	LMRCKQDSDCLAGSVC**LHYSYPVTGP**FCG
S22E10	LMRCKQDSDCLAGSVC**GSRAYPGAAI**FCG
S22E11	LMRCKQDSDCLAGSVC**IYSYPVTEQQ**FCG
S22E12	LMRCKQDSDCLAGSVC**PLAYPLPQSE**FCG

FIGURE 5: (A) Sequences of random clones from the Min-23 library before the selection. (B) Sequences of clones after three rounds of selection on the antibody anti-AMA-1, clone 5G8 (5G8 Ab). Clones R2, R8, R9, and S22E2 have loops of different lengths. Periods (.) represent stop codons. These variations have been introduced by PCR during the cloning process. Randomized positions are shown as bold letters. The known consensus sequence, AYP, is displayed in red, and the new consensus sequence, SYP, is displayed in blue.

were sequenced, and indeed, the consensus sequence AYP was present in seven clones and the homologous sequence SYP in the others (Figure 5).

These results show that the Min-23-R10 library comprised a wide diversity of sequence variation in the surface loop and that specific known binding sequences can be easily and efficiently selected. Figure 5 also shows nine unique sequences of clones randomly picked from the library before the selection. Comparison of Figure 5A and Figure 5B shows that there was no bias in clones before selection against 5G8 Ab and that specific binding clones were easily selected in three rounds of selection. Furthermore, the consensus AYP/SYP sequences identified after the selection were flanked by a variable number of random amino acids on each side, further confirming the diversity of the library (Figure 5).

Six other protein antigens were then used as targets to select new binders from the library, including the malaria apical membrane protein 1 (AMA-1), the mitochondrial membrane protein Tom70, the anti-EBV antibody (anti-EBV Ab), the anti-AMA-1 antibody 1F9 (to compare with selection against 5G8 Ab as described above), the HIV viral protein Nef, and an anti-Nef 15 antibody. After the third and fourth rounds of selection on each target, a significant enrichment of the phage was detected as represented by the ratio of output phage/input phage (Figure 6). Clones were randomly picked from the selected fraction and used for small-scale preparation of phage. Binding was assessed by phage ELISA (Figure 7), and positive binders were sequenced and identified as unique clones (Table 1). The number of positive clones after three or four rounds of

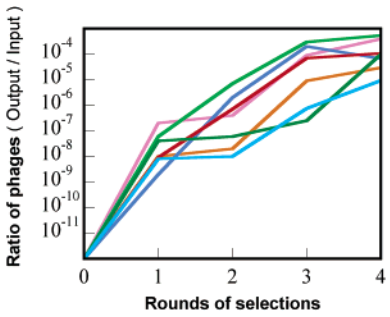

FIGURE 6: Ratio of phage (output phage/input phage) after one, two, three, or four rounds of selection of the library Min-23-R10 on different targets: anti-AMA-1 antibody clone 1F9 (1F9 Ab), purple; clone 5G8 (5G8 Ab), dark blue; AMA-1, red; Tom70, orange; anti-EBV Ab, dark green; anti-Nef Ab, light green; HIV-1 Nef, light blue.

selection was variable for each antigen (Table 1) with a total of 21 different clones isolated for six different targets.

Selected binders were expressed on phage and tested for binding on different targets and on control proteins in ELISA to check the specificity. Representative data of clone S66E1 shows specific binding to the target antibody 1F9 compared to background binding to BSA, antibody anti-His, or antibody anti-HA (Figure 8). Similar specificity was observed for other selected peptides, for example, clone S42E6 binds specifically to the target anti-EBV Ab, clones S40E5, S40E7, S40E9, S40E10, S40E34, and S40E38 bind specifically to Tom70, clones S64E1 and S84E1 bind specifically to AMA-1, clones S66E1, S66E2, S66E4, S66E8, and S66E18 bind specifically to 1F9 Ab, clones S45E1, S45E2, S45E6, and S45E9 bind specifically to anti-Nef Ab, and clone S65E1 binds specifically to Nef (data not shown).

Analysis of Binders (Competition). To further elucidate the binding characteristics of selected clones to their targets, competition experiments were performed by incubation of the selected clones with known ligands for 30 min in solution, prior to ELISA analysis on immobilized targets. For example, the binding of clones S64E1 and S84E1 to AMA-1 was competed by the two ligands previously known to bind AMA-1, the 5G8 antibody and the 1F9 antibody (Figure 9A). The ELISA results demonstrate that 1F9 Ab was able to compete with the binding of both clones S64E1 and S84E1 but no competition was observed with 5G8 Ab. This indicates that clones S64E1 and S84E1 are binding on the same overlapping epitope surface as 1F9 Ab on the AMA-1 protein.

In a reciprocal experiment, the six different clones selected on 1F9 Ab were competed with the natural ligand AMA-1. One representative result for clone S66E1 is depicted in Figure 9B. Indeed, competition for binding on 1F9 Ab was observed when AMA-1 was added to each of the six selected clones, S66E1, S66E2, S66E4, S66E8, S66E17, and S66E18, indicating that all these clones bind on the 1F9 antibody with epitope surfaces overlapping the AMA-1 binding epitope.

In other examples, S42E6 was tested by ELISA for binding to the immobilized anti-EBV antibody while in competition with the natural target, the Epstein Barr Virus (EBV) protein. However, no competition was detected (data not shown) indicating that clone S42E6 apparently binds anti-EBV Ab on a different epitope from that recognized by the EBV protein.

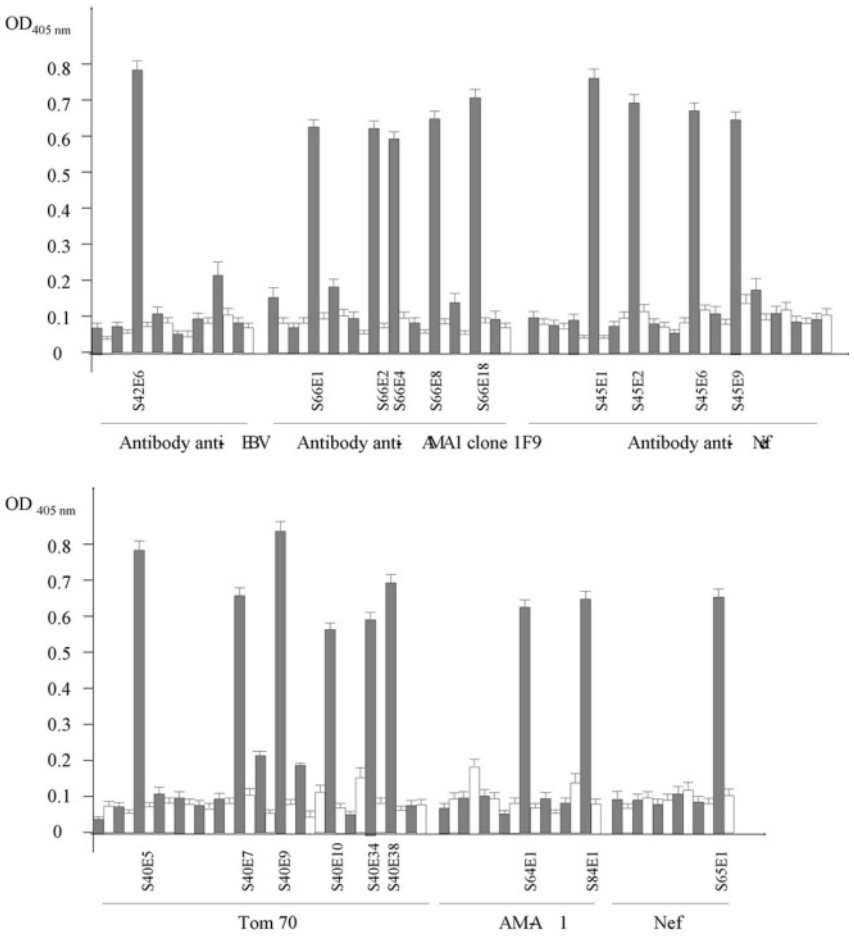

FIGURE 7: Analysis of binding of selected clones by ELISA. Target proteins (gray) and BSA (white) were immobilized, and selected clones expressed on phage were incubated. Bound phage were detected with an HRP-conjugated anti-M13 antibody. Experiments were performed in duplicate, and error bars represent ±standard deviations.

Table 1: Selection of the Min-23-R10 Library on Different Targets[a]

target	abbreviation	target concentration for panning (μg/mL)	number of selection rounds	positive clones isolated
anti-apical membrane(AMA-1) antibody clone 5G8	5G8 Ab	2.5	3	14 (2 consensus sequences)
anti-apical membrane (AMA-1) antibody clone 1F9	1F9 Ab	5	4	5
apical membrane protein-1	AMA-1	10	4	2
mitochondrial membrane protein Tom70	Tom70	10	4	6
anti-Epstein Barr Virus (EBV) antibody	anti-EBV Ab	5	4	1
anti-Nef antibody	anti-Nef Ab	5	4	6
HIV-1 Nef	Nef	5	4	1

[a] Target concentration for panning, number of selection rounds, and number of positive clones isolated.

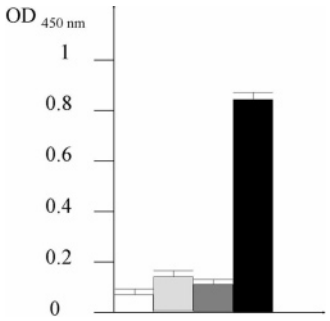

FIGURE 8: Specificity of binding of clone S66E1 on 1F9 antibody analyzed by ELISA. Target proteins (BSA, white; antibody anti-His, light gray; antibody anti-HA, dark gray; antibody anti-AMA-1 (1F9 Ab), black) were immobilized and were incubated with clone S66E1 expressed on phage. Bound phage were detected with an HRP-conjugated anti-M13 antibody. Experiments were performed in duplicate, and error bars represent ±standard deviations.

Similarly, the six clones (S45E1, S45E2, S45E6, S45E8, S45E9, and S45E12) that had been selected on the antibody anti-Nef were tested in competition with the Nef protein. There was no disruption of the binding for any clone indicating that all six selected Min-23 variants bind the anti-Nef Ab using different epitope surfaces from that recognized by Nef. In a reciprocal experiment, the single clone (S65E1) selected on the protein Nef was competed effectively with anti-Nef Ab (data not shown), indicating that they are binding to overlapping epitopes on Nef.

Assessment of Binding Affinity by Surface Plasmon Resonance (Biacore). To confirm that the ELISA binding analysis and competition experiments described above were an accurate representation of the properties of the Min-23 variants, several variants expressed in fusion with MBP were purified and their binding kinetics assessed on immobilized targets using surface plasmon resonance (Biacore). Min-23

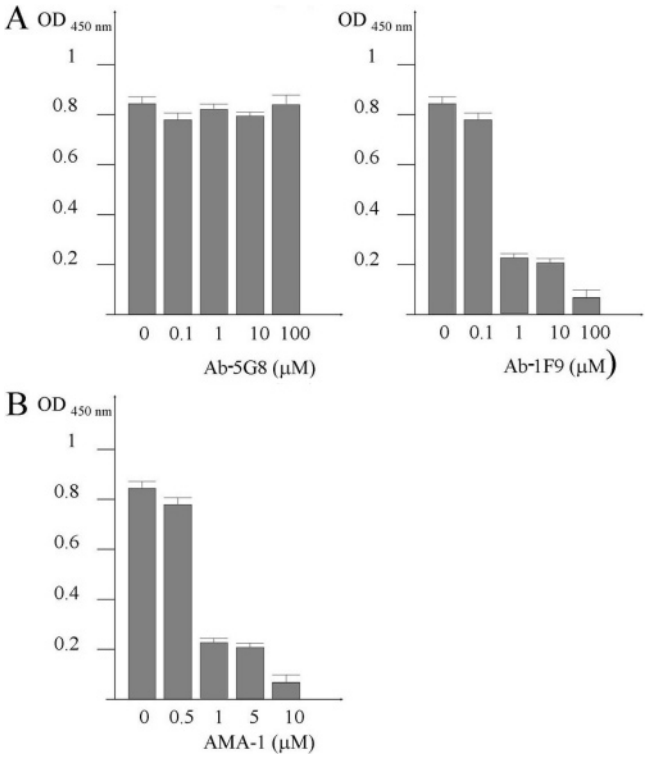

FIGURE 9: (A) Competition of binding of selected clones S64E1 with the anti-AMA-1 antibodies clone 1F9 (1F9 Ab) and clone 5G8 (5G8 Ab). The protein AMA-1 was immobilized and was incubated with selected clone S64E1 expressed on phage, previously mixed with different concentrations of 1F9 Ab and 5G8 Ab. After several washes, bound phage were detected with an HRP-conjugated anti-M13 antibody. Experiments were performed in duplicate, and error bars represent ±standard deviations. Clone S84E1 gave similar results. (B) Competition of binding of selected clone S66E1 with AMA-1 by ELISA. The 1F9 Ab, was immobilized and was incubated with selected clone S66E1 expressed on phage, previously mixed with different concentrations of AMA-1 protein. After several washes, bound phage were detected with an HRP-conjugated anti-M13 antibody. Experiments were performed in duplicate, and error bars represent ±standard deviations.

Table 2: Apparent Kinetic Rate and Equilibrium Binding Constants for the Interaction of S42E6−MBP with Immobilized AntiEBV Antibody[a]

k_a (M^{-1} s^{-1})	k_d (s^{-1})	K_D (M)
3.93×10^4	6.11×10^{-4}	1.55×10^{-8}

[a] The kinetic rate constants k_a and k_d were determined at each of the five concentrations (12.3−204 nM) using the fitting algorithm for 1:1 Langmuir binding (simultaneous fitting of k_a and k_d) model as described in BIAevalution 3.0.2.

variants fused to MBP were tested in parallel with the recombinant MBP protein. As an example, S42E6 binding was assessed against immobilized anti-EBV antibody resulting in kinetics of K_D of 1.55×10^{-8} M as described in Table 2. S42E6 binding was also assessed against immobilized unrelated antibody and no signal was detected.

Relevance of Disulfide Bridges As Assessed by Sensitivity to DTT. To determine if the binding of the selected clones to their target was dependent on the formation of the structurally important disulfide bridges of Min-23, we tested the binding both before and after reduction with dithiotreithol (DTT). For this experiment, prior to analysis by ELISA, each clone was incubated for 30 min with different concentrations

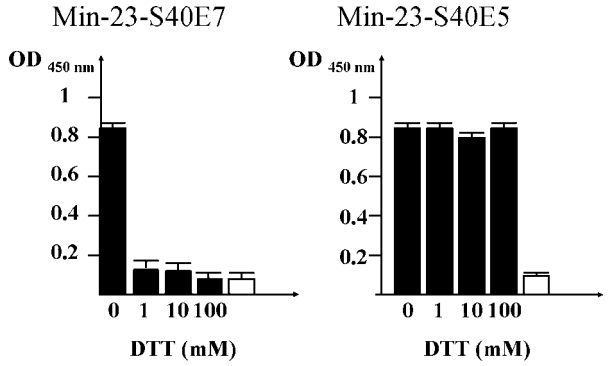

FIGURE 10: Sensitivity of binders to reduction of disulfide bridges by dithiothreitol (DTT). The protein Tom70 was immobilized and was incubated with selected clone S40E5 and S40E7 expressed on phage, previously mixed with different concentrations of DTT. After several washes, bound phage were detected with an HRP-conjugated anti-M13 antibody. Experiments were performed in duplicate, and error bars represent ±standard deviations.

of DTT, as described on the representative graph in Figure 10 for the S40E7 and S40E5 clones. Interestingly, the binding of clone S40E7 to Tom70 is affected by DTT, whereas the binding of clone S40E5 remains unmodified even in the presence of 100 mM DTT. These data indicate that S40E7 might require the stable Min-23 core scaffold for presentation of the predominant binding loop, whereas S40E5 does not have this dependence. Results for all clones are summarized in Table 3. Among the 19 specific clones isolated, 9 clones are sensitive to DTT for binding to their targets, clearly indicating that these clones require at least the presence of the stabilizing disulfide bridges. The remaining 10 clones apparently do not need the disulfide bridges for their binding, which might reflect the display of short linear-peptide sequences that are capable of binding to the target.

Molecular Modeling. Three-dimensional models of several selected clones for which disulfide bridges are important for binding and which are thus folded were built to provide additional information on the selected sequences. In all cases, it was assumed that the folding of the Min-23 scaffold is conserved in the clones as well as the disulfide pairing, and identical to the disulfide pairing in the CSB motif of EETI-II. This was indeed the case for a chimeric peptide obtained by grafting an exogenous loop onto Min-23 (*40*). Conservation of the Min-23 scaffold is likely to imply a disulfide pairing similar to the one in Min-23 and EETI-II. It is worth noting, however, that all cysteines are close to each other in these compounds, and whether proven that, in particular cases, different disulfide pairing could occur within the same structural framework. This ambiguity led to the probably erroneous proposal that the disulfide connectivity of kalata B1 would be I−II, III−VI, and IV−V (*56*) rather than the I−IV, II−V, and III−VI connectivity, specific of knottins (*57*, *58*). Also, it has been shown that modification of the cysteine pairing in another small disulfide-rich protein, maurotoxin, did not markedly alter the scaffold (*59*). Therefore, although unlikely, it cannot be ruled out that some clones adopt a similar fold but different disulfide pairings or even different folds and different disulfide bridges. A three-dimensional representation of clone S40E7 (Tom70 binder) is displayed in Figure 11.

Table 3: Sequences of Selected Clones and Sensitivity of Their Binding to Reduction of Disulfide Bridges by DTT

Target	Clone	Sequence	DTT sensitivity
5G8 Ab		See Figure 5B	ND[a]
1F9 Ab	S66E1	LMRCKQDSDCLAGSVC**RLHGSWWPYP**FCG	+
	S66E2	LMRCKQDSDCLAGSVC**LPYLAWLPSQ**FCG	+
	S66E4	LMRCKQDSDCLAGSVC**RLQELWDVHT**FCG	+
	S66E8	LMRCKQDSDCLAGSVC**RIPAAWFSSA**FCG	+
	S66E18	LMRCKQDSDCLAGSVC**RLEAAWLPLP**FCG	+
AMA-1	S64E1	LMRCKQDSDCLAGSVC**VSPSWWRGPL**FCG	-
	S84E1	LMRCKQDSDCLAGSVC**RLPPLPLWPG**FCG	+
Tom70	S40E5	LMRCKQDSDCLAGSVC**QFHVAFWWPA**FCG	-
	S40E7	LMRCKQDSDCLAGSVC**ASVWWLGPVR**FCG	+
	S40E9	LMRCKQDSDCLAGSVC**MYTLWPSYGR**FCG	-
	S40E10	LMRCKQDSDCLAGSVC**SFEFFPRFGF**FCG	-
	S40E34	LMRCKQDSDCLAGSVC**RFAKRWPPVR**FCG	-
	S40E38	LMRCKQDSDCLAGSVC**LQVWWLGPVR**FCG	-
Anti-Nef Ab	S45E1	LMRCKQDSDCLAGSVC**IKPVFG.VQA**FCG	-
	S45E6	LMRCKQDSDCLAGSVC**IHPLFGFRPS**FCG	-
	S45E2	LMRCKQDSDCLAGSVC**VHPVFAIPWG**FCG	-
	S45E8	LMRCKQDSDCLAGSVC**ARPFFGMFEG**FCG	-
	S45E9	LMRCKQDSDCLAGSVC**YSGITMLPYN**FCG	-
	S45E12	LMRCKQDSDCLAGSVC**VGWPYVYSKG**FCG	-
Nef	S65E1	LMRCKQDSDCLAGSVC**TQVLSFVPWK**FCG	+

[a] ND = not determined.

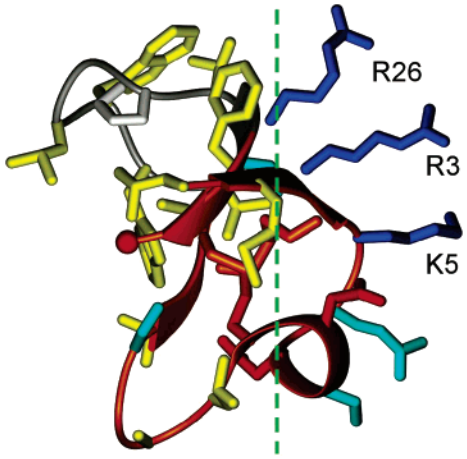

FIGURE 11: Three-dimensional model of clone S40E7 selected for binding to Tom70. The Min-23 scaffold is shown as orange coils, ribbons (3_{10} helix), and arrows (β-strand). The backbone of the inserted and randomized loop is shown as white ribbons. Side chains are color-coded according to the following scheme: hydrophobic, yellow; polar, cyan; acidic, red; basic, blue; proline, white. The C-terminus is shown as a red sphere. The green dashed line highlights the amphiphilic feature. On the right of the line, residues 3, 5, and 26 form a positively charged cluster.

DISCUSSION

In this study, we investigated whether the CSB motif could be manipulated to obtain new binding reagents using the small, well-defined Min-23 peptide, extracted from the squash trypsin inhibitor EETI-II, as a scaffold. A previous report using full EETI-II as a scaffold described the insertion of new sequences in the first loop of EETI-II (*34*), that is, loop "a" according to the knottin nomenclature (*33*). Additional sequences were introduced in EETI-II, and fusion proteins were successfully expressed, suggesting that loop "a" could be used for construction of large libraries. In this study, we chose a different strategy using the elementary structural motif of EETI-II, Min-23, that contains only two out of the three disulfide bridges in EETI-II and is one of the smallest scaffolds reported to date. On the basis of structural analyses and sequence alignments, we inserted residues in the second β-turn of Min-23. This loop, labeled "e" according to the knottin nomenclature, shows a great sequence variability in knottins and other CSB-containing proteins (http://knottin.cbs.cnrs.fr) as represented in Figure 12.

Structural analysis of loop "e" in knottins clearly shows that this loop adopts β-hairpin conformations with both ends of the loop being involved in the conserved antiparallel β-sheet locked by disulfide bridges (Figure 1). We thus hypothesized that this loop would be an appropriate permissive site for introduction of new β-hairpin-like sequences and decided to replace residues 17−20 with a molecular repertoire (Figure 1). First, well-characterized loop sequences, either the 9-residue haemagglutinin (HA) (*52*) or the 17-residue (E-tag) (*53*) was inserted into the β-turn of Min-23. These Min-23 loop insertion mutants were expressed both on phage and as soluble proteins in the periplasm of *E. coli*. Similarly to wild-type Min-23, the loop insertion

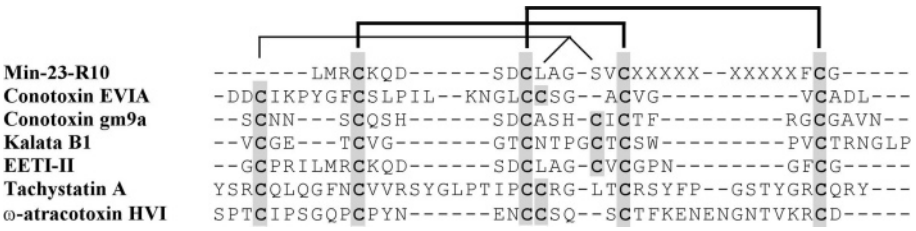

FIGURE 12: Alignment of the sequence of the Min-23-R10 library with other knottin sequences. The disulfide connectivity in Min-23-R10 is shown as thick lines and gray shaded boxes. The additional disulfide bridge in knottins is shown as thin lines.

mutants were well-expressed in *E. coli* (Figure 4). Importantly, loop sequences were capable of binding their respective anti-HA or anti-E antibodies (Figure 3). Together, these results demonstrate that the selected β-turn of Min-23 is permissive for insertion and display of new loop sequences.

To then evaluate the use of Min-23 as a library scaffold, we constructed a Min-23 repertoire (Min-23-R10) comprising 10 random amino acids in the β-turn (Figure 1). A 10-residue loop corresponds to the upper range of loop sizes in the knottin family (*33*) and has previously been shown to be compatible with correct folding (*59*). Specifically, the homologous "e" loop in naturally occurring knottins is 10 residues in length in tachystatin A from horseshoe crab (*60*) and 13 residues in atracotoxin-Hv1a from funnel-web spider (*61*) as represented in Figure 12. It is worth repeating that a chimera in which residues 17−20 were chemically replaced by 10 empirically selected residues was previously shown to fold in a native-like fashion (*40*).

The Min-23-R10 repertoire was constructed as a phage display library of 2.8×10^8 different clones, representing a fraction of the 10^{13} possible combinations of 10 random residues. Phage libraries are always restricted by transformation but are still the most effective technique for display and selection of Min-23 variants. Library diversity and expression quality were confirmed by analysis of random clones selected from the library (Figure 5A). Selecting against a range of different target molecules, each with different properties, sizes, and potential applications, yielded 21 unique Min-23 variants, each with specific binding properties (Tables 1 and 3).

Clones Selected against Tom70. The Min-23-R10 library was selected on Tom70, a well-characterized mitochondrial membrane protein (*62*). After four rounds of selection, six different clones were isolated: S40E5, S40E7, S40E9, S40E10, S40E34, and S40E38, and the best binder by ELISA, clone S40E7, was selected for detailed analysis. The S40E7 loop sequence has a dominant hydrophobic character (two valines, two tryptophans, and one leucine) and can be modeled as a amphiphilic structure with the charged arginine in close contact to the two other positively charged residues near the Min-23 N-terminus (Figure 11). Together, these residues constitute a positively charged surface region that is complemented by a polar region formed by the 310 helix of Min-23 plus the loop serine. The combination of an amphiphilic character combined with the presence of a positively charged cluster is typical of peptides interacting with membranes (via phosphates) as found in several classes of antimicrobial peptides (*63*). The hydrophobic surface of S40E7 is also consistent with the observation that Tom70 binds to several internal hydrophobic segments of precursor proteins (*64*). Although modeling would suggest that the hydrophobic surface might cause non specific aggregation, analyses of binding data reveal that S40E7 is indeed functionally active and folded correctly. Importantly, S40E7 was also shown to be dependent on stable disulfides since it was inactivated by DTT treatment (Table 3).

S40E7 also comprised the Gly−Pro (GP) dipeptide which is frequently observed in β-turns and surface loops and is indeed present in the native Min-23 structure (as GPNG in EETI-II) (Figures 1 and 11). Further, a combinatorial library of EETI-II randomized at GPNG had revealed that the sequence of this turn is significantly constrained and that only the native GPNG sequence provides a high yield in the native fold (*65*). Also, inserting GPNG in the homologous CMTI-III CSB motif significantly improved the chemical synthesis yield (*66*). GP dipeptides can be found in many spider toxins homologous to the same structural knottin family as EETI-II (*33*). Thus, the GP dipeptide in the randomized loop may have been selected for structural and folding reasons in the context of the Min-23 scaffold as a CSB motif.

Clones S64E1 and S84E1 Selected on the AMA-1 Target. The apical membrane antigen 1 (AMA-1) protein is present at the surface of *Plasmodium falciparum* merozoites and is involved in erythrocyte invasion (*67*, *68*). After the selection of the Min-23-R10 library on AMA-1, two different clones were obtained: S64E1 and S84E1. The S64E1 clone comprises the GP dipeptide and, as discussed above for S40E7, this is characteristic of Min-23 with a knottin-fold. Of two tryptophan residues, one appears buried by contacts with the core of the molecule while the second is more solvated and adjacent to the surface arginine. The model also shows that the two prolines face each other in the hairpin loop (data not shown). This arrangement precludes potential extension of the β-sheet toward the tip of the loop that would have generated a regular β-hairpin. It is likely that the prolines participate in the determination of the loop conformation and are important for folding. We have observed that prolines are frequent in the selected sequences from the Min-23-R10 library, similar to the high proline content in loops of natural knottins (*33*).

Examination of the sequences of the selected clones (Table 3) shows that one arginine is present at position 17 in seven clones selected on four different targets. Interestingly, the three-dimensional model of S84E1 (not shown), a clone selected on AMA-1 and sensitive to DTT, suggests that the arginine 17 (the first residue in the randomized loop) might stabilize the peptide fold by making a salt-bridge with the Min-23 C-terminus. A similar stabilization is found in several squash trypsin inhibitors in which an arginine at or near the N-terminus makes a salt-bridge with the C-terminus providing a kind of electrostatic "macrocyclization" similar to the

true peptide macrocyclization observed in squash inhibitors from *Momordica cochinchinensis* (*69*, *70*).

In contrast to clones selected on the anti-AMA1 1F9 Ab, all six clones selected on the anti-Nef Ab are insensitive to the presence of DTT. Thus, whereas the structural constraints afforded by the scaffold appeared favorable for binding to the 1F9 Ab, it seems that no structural constraints were necessary for binding to the anti-Nef Ab, as expected for a target binding a linear peptide (the anti-Nef Ab binds to an N-terminal poorly structured region of the Nef protein (residues 31−50)).

Finally, the one clone selected on Nef, clone S65E1 (Table 3), is not sensitive to competition with the natural target (EBV protein) and thus binds to a different epitope from that of the natural target.

Min-23, a New Small Scaffold for Structurally Constrained Molecular Repertoires. Of the 21 specific binders that were selected against several targets, 12 were DTT insensitive and therefore predicted to display linear epitope loops for which no structural constraints are necessary for binding. Nine clones were DTT sensitive, indicating conformation-dependent binding (Table 3). We are confident that the Min-23 library contains binders with different structural characteristics, combining the advantages of linear peptide libraries and structurally constrained libraries. We are also confident that the CSB fold and cysteine pairing in the conformation-dependent clones are likely to be identical to those of wild-type Min-23. Interestingly, preliminary results on a chemically synthesized peptide corresponding to clone S65E1 indicate that this Min-23 variant displays native-like fold and disulfide bridges (D. Le-Nguyen and A. Heitz, personal communication). Furthermore, an exogenous loop chemically grafted onto the Min-23 scaffold in an identical position and residue size to the Min-23 library (Figure 1) was shown by structural analysis not to perturb the core CSB scaffold (*40*). Clearly, further chemical characterization and structural analyses remain to be performed to definitively assess the disulfide connectivity in all selected Min-23 binders. Correct disulfide bonding is the expected display conformation since many larger proteins have been shown to retain correct disulfide pairing on fd-phage, for example, EGF (three disulfide bridges) (*71*), AMA-1 (eight disulfide bridges) (*55*), or MTI-2 (four disulfide bridges) (*72*). Many even larger protein scaffolds have been effectively displayed in functionally active conformation, including antibody Fab fragments (60 kDa) (*73*), minibodies (*74*), alkaline phosphatase (121 kDa) (*75*), interleukin 1β (17 kDa) (*35*), lysozyme (15 kDa) (*76*), anticalins (17 kDa) (*77*), and Protein A (7 kDa) (*14*).

To extend the concept of peptide library diversity, an innovative report described the simultaneous selection of 22 phage libraries mixed together, comprising both constrained and unconstrained peptides (*78*). The selection on insulin-like growth factor-1 (IGF-1) isolated a dominant single-disulfide scaffold, CX_9C, and yielded an antagonist peptide (*78*). The Min-23 scaffold described here offers an improvement over peptide libraries, because the conserved protein core and the additional disulfide bridge are expected to confer well-defined structural constraints and high stability to the selected binders. Such preferred protein scaffolds have high intrinsic stability able to induce geometrical constraints on inserted peptide loops (*11*, *12*, *35*). Indeed, since Min-23 displays high intrinsic stability (*39*), the core sequence is conserved in the Min-23-R10 library, and fold conservation has been verified on two examples (clone S65E1 and the Min-23-RT chimera); Min-23 can be claimed to be a validated scaffold.

Other small scaffolds have been recently displayed on fd-phage, including alpha-conotoxin (*10*), although the structure and cysteine pairing in the selected binders were not determined, and the 36-residue cellulose binding domain (CBD) (*21*, *22*). The CBD scaffold is slightly larger than it is in Min-23 and significantly differs both in size, conformation, and randomization strategy. Our Min-23-R10 library was particularly suited to display exposed but stabilized β-hairpins (*40*). A different peptide scaffold has been designed with a single-disulfide bridge and an optimized β-hairpin sequence (*79*), but (i) has not yet been used in phage display selection, (ii) is expected to be less stable than Min-23, and (iii) appears useful for display of β-turns rather than of β-hairpins since the β-hairpin itself is part of the scaffold.

The small size of the Min-23 scaffold presents a number of potential advantages such as simple chemical synthesis and manipulation, better tissue penetration for in vivo targeting, and enhanced penetration of clefts and cavities in target antigens. These features generate numerous clinical diagnostics and therapeutic applications, especially to bind immunosilent (buried) epitopes which cannot be accessed by larger proteins such as the natural immune repertoire. Small protein domains are ideal for in vivo imaging and intracellular targeting applications. Besides, in contrast to immunoglobulins, small disulfide-rich scaffolds consist of a single polypeptide chain, which makes cloning and recombinant expression easier. Our selected Min-23 variants may have practical applications; the malarial apical membrane antigen-1 (AMA-1) is expressed on the surface of merozoites, has a role in erythrocytes attachment prior to parasite invasion (*55*), and is a potential vaccine candidate (*80*). Selection of AMA-1 binders and/or AMA-1 mimotopes provides high-value reagents in the development of effective vaccines directed against *Plasmodium falciparum*. Two monoclonal antibodies are available which recognize both recombinant refolded *Plasmodium falciparum* AMA-1 and the native molecule expressed in parasite; 5G8 Ab binds to a linear epitope of AMA-1, whereas 1F9 Ab recognizes a conformational epitope (*55*). We have isolated Min-23 variants that either (a) bind to AMA-1 as antibody mimetics or (b) bind to 5G8 Ab and 1F9 Ab and are therefore AMA-1 mimetics. It would be interesting to evaluate these monovalent Min-23 variants in comparison to the larger, bivalent parent antibodies or the AMA-1 antigen in various clinical applications. The emergence of HIV-1 drug resistance renders the development of new drugs crucial for improved HIV treatments. HIV-1 Nef, an accessory protein with important roles in HIV pathogenicity, is an important drug target (*81*). We have isolated a Min-23 variant that binds to HIV-1 Nef and could potentially be formulated as a biopharmaceutical. Such small, rapidly targeting and rapidly penetrating Min-23 reagents could offer significant advantages over the larger immunoglobulin V-like reagents derived from mammals, camelids, or sharks. Moreover, since Min-23 variants are amenable for chemical synthesis, simple modifications can be introduced to reduce immunogenicity or improve bioavailability. For novel applications, small

targeting molecules are of great interest as they can penetrate clefts and enzyme active sites. For example, the thrombin molecule exhibits an unusual deep and narrow active site cleft, which is the major determinant for its restricted substrate specificity (*82*). A small 46-residue scaffold library of the tryptase inhibitor (LDTI) was selected on thrombin and a low-affinity thrombin inhibitor isolated (*82*). Min-23 variants are potentially an alternative thrombin inhibitor. Interestingly, the Min-23 scaffold is based on the structural motif of knottins, and one naturally occurring circular knottin, kalata B1, is the orally active component of a plant decoction used in traditional African medicine (*83*). Circular knottins display remarkable thermal stability and resistance to exo- and endoproteases, and chemical routes to synthesis of circular knottins are now available (*84*−*86*). Therefore, any Min-23 variant selected against a high-value target could be stabilized as a circular knottin.

CONCLUSION

Our success in isolating binders from the Min-23 library on a range of very different targets indicates that Min-23 represents one of the smallest known scaffolds for efficient phage display and selection. We have shown that the Min-23-R10 library complements antibody repertoires and provides a novel application of the CSB motif as a template to create novel proteins. This study was a proof of principle clearly demonstrating the potential of the CSB scaffold for derivation of a structurally constrained random library and selection of new binders. We have shown that, in many cases, formation of the disulfide bridges is a requisite for target binding indicating that the Min-23 variants are structurally folded. Although modeling provided some structural insights, more detailed analyses should await chemical synthesis and structural analysis of many Min-23 variants to (i) determine the precise effect of inserted loops on the structural scaffold, (ii) elucidate the structural constraints imposed by the CSB scaffold, and, ultimately, (iii) obtain information on binding surface dynamics at the atomic level. This information will, in turn, be used to create more complex libraries for the selection of novel binding reagents beyond the current limitations inherent to larger protein scaffolds. The new structured peptide ligands discovered in this study will bind pharmacological important targets such as the HIV Nef protein or the *Plasmodium falciparum* AMA-1 and may constitute interesting lead compounds in future drug development.

ACKNOWLEDGMENT

We thank Nick Hoogenraad for providing the Tom70 protein, Mick Foley for providing the AMA-1 protein, Robin Anders for providing the antibodies 5G8 and 1F9, and Olan Dolezal and Meghan Hattarki for helping with Biosensor experiments. We thank Annie Heitz and Anne Nathanielsz for their help in finalizing this manuscript.

REFERENCES

1. Vaughan, T. J., Williams, A. J., Pritchard, K., Osbourn, J. K., Pope, A. R., Earnshaw, J. C., McCafferty, J., Hodits, R. A., Wilton, J., and Johnson, K. S. (1996) Human antibodies with subnanomolar affinities isolated from a large non-immunized phage display library, *Nat. Biotechnol. 14*, 309−314.
2. Clackson, T. P. (1991) Genetically engineered monoclonal antibodies, *Br. J. Rheumatol. 2*, 36−39.
3. Hoogenboom, H. R., and Chames, P. (2000) Natural and designer binding sites made by phage display technology, *Immunol. Today 21*, 371−378.
4. Scott, J. K., and Craig, L. (1994) Random peptide libraries, *Curr. Opin. Biotechnol. 5*, 40−48.
5. Cwirla, S. E., Peters, E. A., Barrett, R. W., and Dower, W. J. (1990) Peptides on phage: a vast library of peptides for identifying ligands, *Proc. Natl. Acad. Sci. U.S.A. 87*, 6378−6382.
6. Zwick, M. B., Shen, J., and Scott, J. K. (1998) Phage-displayed peptide libraries, *Curr. Opin. Biotechnol. 9*, 427−436.
7. Lu, Z., Murray, K. S., Van Cleave, V., LaVallie, E. R., Stahl, M. L., and McCoy, J. M. (1995) Expression of thioredoxin random peptide libraries on the *Escherichia coli* cell surface as functional fusions to flagellin: a system designed for exploring protein−protein interactions, *Biotechnology (NY) 13*, 366−372.
8. Koivunen, E., Wang, B., and Ruoslahti, E. (1995) Phage libraries displaying cyclic peptides with different ring sizes: ligand specificities of the RGD-directed integrins, *Biotechnology (NY) 13*, 265−270.
9. Wrighton, N. C., Farrell, F. X., Chang, R., Kashyap, A. K., Barbone, F. P., Mulcahy, L. S., Johnson, D. L., Barrett, R. W., Jolliffe, L. K., and Dower, W. J. (1996) Small peptides as potent mimetics of the protein hormone erythropoietin, *Science 273*, 458−464.
10. Bonnycastle, L. L., Mehroke, J. S., Rashed, M., Gong, X., and Scott, J. K. (1996) Probing the basis of antibody reactivity with a panel of constrained peptide libraries displayed by filamentous phage, *J. Mol. Biol. 258*, 747−762.
11. Nygren, P. A., and Uhlen, M. (1997) Scaffolds for engineering novel binding sites in proteins, *Curr. Opin. Struct. Biol. 7*, 463−469.
12. Skerra, A. (2000) Engineered protein scaffolds for molecular recognition, *J. Mol. Recognit. 13*, 167−187.
13. Braisted, A. C., and Wells, J. A. (1996) Minimizing a binding domain from protein A, *Proc. Natl. Acad Sci. U.S.A. 93*, 5688−5692.
14. Nord, K., Gunneriusson, E., Ringdahl, J., Stahl, S., Uhlen, M., and Nygren, P. A. (1997) Binding proteins selected from combinatorial libraries of an alpha-helical bacterial receptor domain, *Nat. Biotechnol. 15*, 772−777.
15. McConnell, S. J., and Hoess, R. H. (1995) Tendamistat as a scaffold for conformationally constrained phage peptide libraries, *J. Mol. Biol. 250*, 460−470.
16. Markland, W., Ley, A. C., and Ladner, R. C. (1996) Iterative optimization of high-affinity protease inhibitors using phage display. 2. Plasma kallikrein and thrombin, *Biochemistry 35*, 8058−8067.
17. Xu, L., Aha, P., Gu, K., Kuimelis, R. G., Kurz, M., Lam, T., Lim, A. C., Liu, H., Lohse, P. A., Sun, L., Weng, S., Wagner, R. W., and Lipovsek, D. (2002) Directed evolution of high-affinity antibody mimics using mRNA display, *Chem. Biol. 9*, 933−942.
18. Koide, A., Bailey, C. W., Huang, X., and Koide, S. (1998) The fibronectin type III domain as a scaffold for novel binding proteins, *J. Mol. Biol. 284*, 1141−1151.
19. Beste, G., Schmidt, F. S., Stibora, T., and Skerra, A. (1999) Small antibody-like proteins with prescribed ligand specificities derived from the lipocalin fold, *Proc. Natl. Acad. Sci. U.S.A. 96*, 1898−1903.
20. Skerra, A. (2001) 'Anticalins': a new class of engineered ligand-binding proteins with antibody-like properties, *J. Biotechnol. 74*, 257−275.
21. Smith, G. P., Patel, S. U., Windass, J. D., Thornton, J. M., Winter, G., and Griffiths, A. D. (1998) Small binding proteins selected from a combinatorial repertoire of knottins displayed on phage, *J. Mol. Biol. 277*, 317−332.
22. Lehtio, J., Teeri, T. T., and Nygren, P. A. (2000) Alpha-amylase inhibitors selected from a combinatorial library of a cellulose binding domain scaffold, *Proteins 41*, 316−322.
23. Kiczak, L., Kasztura, M., Koscielska-Kasprzak, K., Dadlez, M., and Otlewski, J. (2001) Selection of potent chymotrypsin and elastase inhibitors from M13 phage library of basic pancreatic trypsin inhibitor (BPTI), *Biochim. Biophys. Acta 17*, 153−163.
24. Nuttall, S. D., Rousch, M. J., Irving, R. A., Hufton, S. E., Hoogenboom, H. R., and Hudson, P. J. (1999) Design and expression of soluble CTLA-4 variable domain as a scaffold for the display of functional polypeptides, *Proteins 36*, 217−227.

25. Cicortas Gunnarsson, L., Nordberg Karlsson, E., Albrekt, A. S., Andersson, M., Holst, O., and Ohlin, M. (2004) A carbohydrate binding module as a diversity-carrying scaffold, *Protein Eng., Des. Sel. 17*, 213−221.
26. Otlewski, J., and Krowarsch, D. (1996) Squash inhibitor family of serine proteinases, *Acta Biochim. Pol. 43*, 431−444.
27. Heitz, A., Chiche, L., Le-Nguyen, D., and Castro, B. (1989) ^{1}H 2D NMR and distance geometry study of the folding of *Ecballium elaterium* trypsin inhibitor, a member of the squash inhibitors family, *Biochemistry 28*, 2392−2398.
28. Chiche, L., Gaboriaud, C., Heitz, A., Mornon, J. P., Castro, B., and Kollman, P. A. (1989) Use of restrained molecular dynamics in water to determine three-dimensional protein structure: prediction of the three-dimensional structure of *Ecballium elaterium* trypsin inhibitor II, *Proteins 6*, 405−417.
29. Bode, W., Greyling, H. J., Huber, R., Otlewski, J., and Wilusz, T. (1989) The refined 2.0 Å X-ray crystal structure of the complex formed between bovine beta-trypsin and CMTI-I, a trypsin inhibitor from squash seeds (*Cucurbita maxima*). Topological similarity of the squash seed inhibitors with the carboxypeptidase A inhibitor from potatoes, *FEBS Lett. 242*, 285−292.
30. Le Nguyen, D., Heitz, A., Chiche, L., Castro, B., Boigegrain, R. A., Favel, A., and Coletti-Previero, M. A. (1990) Molecular recognition between serine proteases and new bioactive microproteins with a knotted structure, *Biochimie 72*, 431−435.
31. Pallaghy, P. K., Nielsen, K. J., Craik, D. J., and Norton, R. S. (1994) A common structural motif incorporating a cystine knot and a triple-stranded beta-sheet in toxic and inhibitory polypeptides, *Protein Sci. 3*, 1833−1839.
32. Craik, D. J., Daly, N. L., and Waine, C. (2001) The cystine knot motif in toxins and implications for drug design, *Toxicon 39*, 43−60.
33. Gelly, J. C., Gracy, J., Kaas, Q., Le-Nguyen, D., Heitz, A., and Chiche, L. (2004) The KNOTTIN website and database: a new information system dedicated to the knottin scaffold, *Nucleic Acids Res.*, D156−159.
34. Christmann, A., Walter, K., Wentzel, A., Kratzner, R., and Kolmar, H. (1999) The cystine knot of a squash-type protease inhibitor as a structural scaffold for *Escherichia coli* cell surface display of conformationally constrained peptides, *Protein Eng. 12*, 797−806.
35. Nygren, P. A., and Skerra, A. (2004) Binding proteins from alternative scaffolds, *J. Immunol. Methods 290*, 3−28.
36. Heitz, A., Chiche, L., Le-Nguyen, D., and Castro, B. (1995) Folding of the squash trypsin inhibitor EETI II. Evidence of native and non-native local structural preferences in a linear analogue, *Eur. J. Biochem. 233*, 837−846.
37. Chiche, L., Heitz, A., Padilla, A., Le-Nguyen, D., and Castro, B. (1993) Solution conformation of a synthetic bis-headed inhibitor of trypsin and carboxypeptidase A: new structural alignment between the squash inhibitors and the potato carboxypeptidase inhibitor, *Protein Eng. 6*, 675−682.
38. Le-Nguyen, D., Heitz, A., Chiche, L., el Hajji, M., and Castro, B. (1993) Characterization and 2D NMR study of the stable [9-21, 15-27] 2 disulfide intermediate in the folding of the 3 disulfide trypsin inhibitor EETI II, *Protein Sci. 2*, 165−174.
39. Heitz, A., Le-Nguyen, D., and Chiche, L. (1999) Min-21 and min-23, the smallest peptides that fold like a cystine-stabilized beta-sheet motif: design, solution structure, and thermal stability, *Biochemistry 38*, 10615−10625.
40. Heitz, A., Le-Nguyen, D., Dumas, C., and Chiche, L. (2000) Engineering potential inhibitors of the interaction between the HIV-1 Nef protein and kinase SH3 domains, in *Peptides 2000* (Martinez, J., and Fehrentz, J. A., Eds.) pp 415−416, Editions EDK, Paris.
41. Lilley, G. G., Dolezal, O., Hillyard, C. J., Bernard, C., and Hudson, P. J. (1994) Recombinant single-chain antibody peptide conjugates expressed in *Escherichia coli* for the rapid diagnosis of HIV, *J. Immunol. Methods 171*, 211−226.
42. Griffiths, A. D., Williams, S. C., Hartley, O., Tomlinson, I. M., Waterhouse, P., Crosby, W. L., Kontermann, R. E., Jones, P. T., Low, N. M., Allison, T. J., et al. (1994) Isolation of high affinity human antibodies directly from large synthetic repertoires, *EMBO J. 13*, 3245−3260.
43. Kapust, R. B., and Waugh, D. S. (1999) *Escherichia coli* maltose-binding protein is uncommonly effective at promoting the solubility of polypeptides to which it is fused, *Protein Sci. 8*, 1668−1674.
44. Koradi, R., Billeter, M., and Wuthrich, K. (1996) MOLMOL: a program for display and analysis of macromolecular structures, *J. Mol. Graph. 14*, 51−55, 29−32.
45. Sali, A., and Blundell, T. L. (1993) Comparative protein modelling by satisfaction of spatial restraints, *J. Mol. Biol. 234*, 779−815.
46. Case, D. A., Pearlman, D. A., Caldwell, J. W., Cheatham, T. E., Wang, J., Ross, W. S., Simmerling, C. L., Darden, T. A., Merz, K. M., Stanton, R. V., Cheng, A. L., Vincent, J. J., Crowley, M., Tsui, V., Gohlke, H. V., Radmer, R. J., Duan, Y., Pitera, J., Massova, I., Seibel, G. L., Singh, U. C., Weiner, P. K., and Kollman, P. A. (2002) Amber 7, University of California, San Francisco, CA.
47. Cornell, W. D., Cieplak, P., Bayly, C. I., Gould, I. R., Merz, K. M., Jr, Ferguson, D. M., Spellmeyer, D. C., Fox, T., Caldwell, J. W., and Kollman, P. A. (1995) A second generation force field for the simulation of proteins and nucleic acids, *J. Am. Chem. Soc. 117*, 5179−5197.
48. Cornell, W., Abseher, R., Nilges, M., and Case, D. A. (2001) Continuum solvent molecular dynamics study of flexibility in interleukin-8, *J. Mol. Graphics Modell. 19*, 136−145.
49. Tsui, V., and Case, D. A. (2000) Molecular dynamics simulations of nucleic acids with a Generalized Born solvation model, *J. Am. Chem. Soc. 122*, 2489−2498.
50. van Gunsteren, W. F., and Berendsen, H. J. C. (1977) Algorithms for macromolecular dynamics and constraints dynamics, *Mol. Phys. 34*, 1311−1327.
51. Berendsen, H. J. C., Postma, J. P. M., van Gunsteren, W. F., DiNola, A., and Haak, J. R. (1984) Molecular dynamics with coupling to an external bath, *J. Chem. Phys. 81*, 3684−3690.
52. Wabuke-Bunoti, M. A., Taku, A., Fan, D. P., Kent, S., and Webster, R. G. (1984) Cytolytic T lymphocyte and antibody responses to synthetic peptides of influenza virus hemagglutinin, *J. Immunol. 133*, 2194−2201.
53. Kiefer, M. C., Saphire, A. C., Bauer, D. M., and Barr, P. J. (1990) The cDNA and derived amino acid sequences of human and bovine bone Gla protein, *Nucleic Acids Res. 18*, 1909.
54. Jellis, C. L., Cradick, T. J., Rennert, P., Salinas, P., Boyd, J., Amirault, T., and Gray, G. S. (1993) Defining critical residues in the epitope for a HIV-neutralizing monoclonal antibody using phage display and peptide array technologies, *Gene 137*, 63−68.
55. Coley, A. M., Campanale, N. V., Casey, J. L., Hodder, A. N., Crewther, P. E., Anders, R. F., Tilley, L. M., and Foley, M. (2001) Rapid and precise epitope mapping of monoclonal antibodies against *Plasmodium falciparum* AMA1 by combined phage display of fragments and random peptides, *Protein Eng. 14*, 691−698.
56. Skjeldal, L., Gran, L., Sletten, K., and Volkman, B. F. (2002) Refined structure and metal binding site of the kalata B1 peptide, *Arch. Biochem. Biophys. 399*, 142−148.
57. Saether, O., Craik, D. J., Campbell, I. D., Sletten, K., Juul, J., and Norman, D. G. (1995) Elucidation of the primary and three-dimensional structure of the uterotonic polypeptide kalata B1, *Biochemistry 34*, 4147−4158.
58. Rosengren, K. J., Daly, N. L., Plan, M. R., Waine, C., and Craik, D. J. (2003) Twists, knots, and rings in proteins. Structural definition of the cyclotide framework, *J. Biol. Chem. 278*, 8606−8616.
59. M'Barek, S., Lopez-Gonzalez, I., Andreotti, N., di Luccio, E., Visan, V., Grissmer, S., Judge, S., El Ayeb, M., Darbon, H., Rochat, H., Sampieri, F., Beraud, E., Fajloun, Z., De Waard, M., and Sabatier, J. M. (2003) A maurotoxin with constrained standard disulfide bridging: innovative strategy of chemical synthesis, pharmacology, and docking on K+ channels, *J. Biol. Chem. 278*, 31095−31104.
60. Fujitani, N., Kawabata, S., Osaki, T., Kumaki, Y., Demura, M., Nitta, K., and Kawano, K. (2002) Structure of the antimicrobial peptide tachystatin A, *J. Biol. Chem. 277*, 23651−23657.
61. Fletcher, J. I., Smith, R., O'Donoghue, S. I., Nilges, M., Connor, M., Howden, M. E., Christie, M. J., and King, G. F. (1997) The structure of a novel insecticidal neurotoxin, omega-atracotoxin-HV1, from the venom of an Australian funnel web spider, *Nat. Struct. Biol. 4*, 559−566.
62. Young, J. C., Hoogenraad, N. J., and Hartl, F. U. (2003) Molecular chaperones Hsp90 and Hsp70 deliver preproteins to the mitochondrial import receptor Tom70, *Cell 112*, 41−50.
63. Hancock, R. E., and Scott, M. G. (2000) The role of antimicrobial peptides in animal defenses, *Proc. Natl. Acad. Sci. U.S.A. 97*, 8856−8861.

64. Chacinska, A., Pfanner, N., and Meisinger, C. (2002) How mitochondria import hydrophilic and hydrophobic proteins, *Trends Cell Biol. 12*, 299−303.
65. Wentzel, A., Christmann, A., Kratzner, R., and Kolmar, H. (1999) Sequence requirements of the GPNG beta-turn of the *Ecballium elaterium* trypsin inhibitor II explored by combinatorial library screening, *J. Biol. Chem. 274*, 21037−21043.
66. Rolka, K., Kupryszewski, G., Ragnarsson, U., Otlewski, J., Krokoszynska, I., and Wilusz, T. (1991) in *Peptides 1990* (Giralt, E., and Andreu, D., Eds.) pp 768−771, ESCOM Science Publishers, Leiden, The Netherlands.
67. Silvie, O., Franetich, J. F., Charrin, S., Mueller, M. S., Siau, A., Bodescot, M., Rubinstein, E., Hannoun, L., Charoenvit, Y., Kocken, C. H., Thomas, A. W., Van Gemert, G. J., Sauerwein, R. W., Blackman, M. J., Anders, R. F., Pluschke, G., and Mazier, D. (2004) A role for apical membrane antigen 1 during invasion of hepatocytes by *Plasmodium falciparum* sporozoites, *J. Biol. Chem. 279*, 9490−9496.
68. Mitchell, G. H., Thomas, A. W., Margos, G., Dluzewski, A. R., and Bannister, L. H. (2004) Apical membrane antigen 1, a major malaria vaccine candidate, mediates the close attachment of invasive merozoites to host red blood cells, *Infect. Immun. 72*, 154−158.
69. Heitz, A., Hernandez, J. F., Gagnon, J., Hong, T. T., Pham, T. T., Nguyen, T. M., Le-Nguyen, D., and Chiche, L. (2001) Solution structure of the squash trypsin inhibitor MCoTI-II. A new family for cyclic knottins, *Biochemistry 40*, 7973−7983.
70. Hernandez, J. F., Gagnon, J., Chiche, L., Nguyen, T. M., Andrieu, J. P., Heitz, A., Trinh Hong, T., Pham, T. T., and Le Nguyen, D. (2000) Squash trypsin inhibitors from *Momordica cochinchinensis* exhibit an atypical macrocyclic structure, *Biochemistry 39*, 5722−5730.
71. Souriau, C., Gracy, J., Chiche, L., and Weill, M. (1999) Direct selection of EGF mutants displayed on filamentous phage using cells overexpressing EGF receptor, *Biol. Chem. 380*, 451−458.
72. Volpicella, M., Ceci, L. R., Gallerani, R., Jongsma, M. A., and Beekwilder, J. (2001) Functional expression on bacteriophage of the mustard trypsin inhibitor MTI-2, *Biochem. Biophys. Res. Commun. 280*, 813−817.
73. de Haard, H. J., van Neer, N., Reurs, A., Hufton, S. E., Roovers, R. C., Henderikx, P., de Bruine, A. P., Arends, J. W., and Hoogenboom, H. R. (1999) A large non-immunized human Fab fragment phage library that permits rapid isolation and kinetic analysis of high affinity antibodies, *J. Biol. Chem. 274*, 18218−18230.
74. Tramontano, A., Bianchi, E., Venturini, S., Martin, F., Pessi, A., and Sollazzo, M. (1994) The making of the minibody: an engineered beta-protein for the display of conformationally constrained peptides, *J. Mol. Recognit. 7*, 9−24.
75. Ladner, R. C., and Ley, A. C. (2001) Novel frameworks as a source of high-affinity ligands, *Curr. Opin. Biotechnol. 12*, 406−410.
76. Vaughan, C. K., and Sollazzo, M. (2001) Of minibody, camel and bacteriophage, *Comb. Chem. High Throughput Screening 4*, 417−430.
77. Schlehuber, S., and Skerra, A. (2002) Tuning ligand affinity, specificity, and folding stability of an engineered lipocalin variant—a so-called 'anticalin'—using a molecular random approach, *Biophys. Chem. 96*, 213−228.
78. Deshayes, K., Schaffer, M. L., Skelton, N. J., Nakamura, G. R., Kadkhodayan, S., and Sidhu, S. S. (2002) Rapid identification of small binding motifs with high-throughput phage display: discovery of peptidic antagonists of IGF-1 function, *Chem. Biol. 9*, 495−505.
79. Cochran, A. G., Tong, R. T., Starovasnik, M. A., Park, E. J., McDowell, R. S., Theaker, J. E., and Skelton, N. J. (2001) A minimal peptide scaffold for beta-turn display: optimizing a strand position in disulfide-cyclized beta-hairpins, *J. Am. Chem. Soc. 123*, 625−632.
80. Anders, R. F., Crewther, P. E., Edwards, S., Margetts, M., Matthew, M. L., Pollock, B., and Pye, D. (1998) Immunisation with recombinant AMA-1 protects mice against infection with *Plasmodium chabaudi*, *Vaccine 16*, 240−247.
81. Murakami, Y., Fukazawa, H., Kobatake, T., Yamagoe, S., Takebe, Y., Tobiume, M., Matsuda, M., and Uehara, Y. (2002) A mammalian two-hybrid screening system for inhibitors of interaction between HIV Nef and the cellular tyrosine kinase Hck, *Antiviral Res. 55*, 161−168.
82. Tanaka, A. S., Silva, M. M., Torquato, R. J., Noguti, M. A., Sampaio, C. A., Fritz, H., and Auerswald, E. A. (1999) Functional phage display of leech-derived tryptase inhibitor (LDTI): construction of a library and selection of thrombin inhibitors, *FEBS Lett. 458*, 11−16.
83. Gran, L., Sandberg, F., and Sletten, K. (2000) Oldenlandia affinis (R&S) DC. A plant containing uteroactive peptides used in African traditional medicine, *J. Ethnopharmacol. 70*, 197−203.
84. Tam, J. P., and Lu, Y. A. (1998) A biomimetic strategy in the synthesis and fragmentation of cyclic protein, *Protein Sci. 7*, 1583−1592.
85. Daly, N. L., Love, S., Alewood, P. F., and Craik, D. J. (1999) Chemical synthesis and folding pathways of large cyclic polypeptides: studies of the cystine knot polypeptide kalata B1, *Biochemistry 38*, 10606−10614.
86. Le-Nguyen, D., Barry, L. G., Tam, J. P., Heitz, A., Chiche, L., Hernandez, J. F., and Pham, T. T. (2003) Synthesis of MCoTI-I, a cyclic trypsin inhibitor from *Momordica Cochinchinensis*, in *Peptides 2002* (Benedetti, E., and Pedone, C., Eds.) pp 182−183, Edizioni Ziino, Napoli, Italy.

BI0481592